Magnetic excitations in amorphous ferromagnets

G. Shirane, J. D. Axe, and C. F. Majkrzak
Brookhaven National Laboratory, Upton, New York 11973

T. Mizoguchi
Gakushuin University, Tokyo, Japan
(Received 12 February 1982)

The magnon excitations near the first $\mathcal{S}(Q)$ maximum in amorphous ferromagnets have been reexamined by the use of a triple-axis polarized-beam spectrometer. This technique permits us to separate inelastic magnetic cross sections from phonons and all elastic components. We point out that this technique is not useful once the magnon excitation energy becomes smaller than the instrumental width. We have examined three different Fe-based alloy compositions at room temperature. In each case our results are consistent with a mechanism involving "umklapp scattered" long-wavelength spin waves with no energy gap. We compare our results on $Fe_{75}P_{15}C_{10}$ with those of Mook and Tsuei who interpreted their results in terms of a 19-meV energy gap in $Fe_{75}P_{15}C_{10}$.

I. INTRODUCTION

The power of polarized neutrons for magnetic studies was amply demonstrated by Moon, Riste, and Koehler in their classic paper on polarization analysis.[1] One application of the technique is the study of magnetic excitations with a polarized incident beam *without* polarization analysis of the scattered beam. If we place a ferromagnet at the sample position in a horizontal magnetic field (parallel to the scattering vector $\vec{Q}$), then the difference of spin-up (+) and spin-down (−) cross sections selects out only the inelastic spin-wave component. This is particularly suitable for the study of amorphous ferromagnets to separate out the nonmagnetic scattering. The technique was successfully applied by Mook *et al.*[2] and by Mook and Tsuei[3] for the study of magnetic excitations in amorphous ferromagnetic alloys, in particular, near the first peak in $\mathcal{S}(Q)$ around $Q_0 \approx 3$ Å^{-1}.

Mook and Tsuei[3] reported a detailed study of $Fe_{75}P_{15}C_{10}$ and their major observations are schematically depicted in Fig. 1(b). They utilize a time-of-flight polarized-beam spectrometer with the correlation technique for a high efficiency of data collection. They have succeeded in observing the dip in magnetic excitation energy near the maximum of $\mathcal{S}(Q)$ and reported a rotonlike gap of 20 meV at room temperature at $Q = Q_0$. Theoretical models[4] have been proposed to explain this type of magnon energy gap.

Recently, we have designed a new polarized-beam spectrometer with a variety of modulation techniques in mind. In the process we carefully reexamined the problems associated with the above polarized-beam technique for inelastic scattering. We came upon the following simple conceptual problem concerning the interpretation of the data.

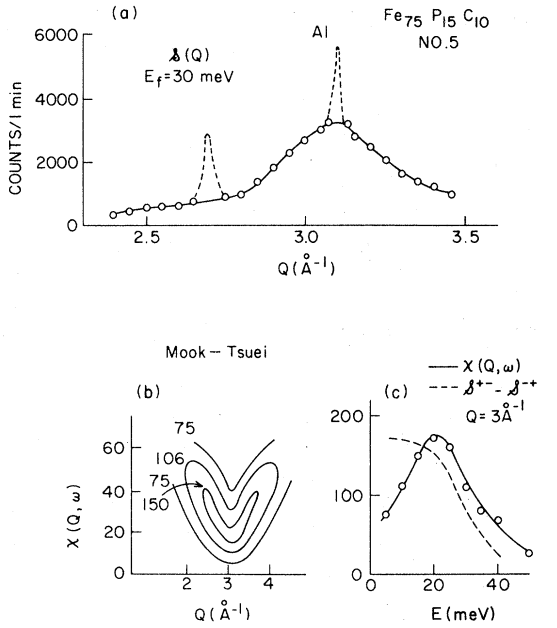

FIG. 1. (a) Maximum of $\mathcal{S}(Q)$ is demonstrated for amorphous ferromagnet $Fe_{75}P_{15}C_{10}$ at room temperature. The data were taken with an analyzer set at 30 meV. Previous magnon data of this compound by Mook and Tsuei (Ref. 3) are schematically shown in (b) and (c); $E_i = 120$ meV.

The measurements consist of taking the difference of counts in the (+) (flipper OFF) and (−) (flipper ON) channels at a given setting of Q and ω. Neglecting magnon-lifetime effects we have $\mathcal{S}^{\pm}\neq 0$ and $\mathcal{S}^{\mp}=0$ for $\omega>0$, while $\mathcal{S}^{\pm}=0$ and $\mathcal{S}^{\mp}\neq 0$ for $\omega<0$. In the limit $\hbar\omega \ll kT$,

$$\mathcal{S}^{\pm}(\omega>0)=\mathcal{S}^{\mp}(\omega<0)$$

so that $\mathcal{S}^{\pm}-\mathcal{S}^{\mp}$ is an odd function of ω. The measured intensity is a convolution of $\mathcal{S}^{\pm}-\mathcal{S}^{\mp}$ with the appropriate instrumental resolution (even in ω) and therefore passes through zero at $\omega=0$. This technique thus will produce a peak at a finite energy even for a gapless excitation spectrum. The peak in this case is essentially determined by the instrumental energy width. This peak can be mistaken as an indication of the magnon energy gap. It appeared to us worthwhile to reexamine the magnetic excitations in amorphous ferromagnets from this particular viewpoint.

This paper reports the measurements on magnetic excitations in the three different amorphous ferromagnets shown in Table I. The spin-wave dispersion of sample 1 at small Q was previously reported by Axe *et al.*,[5] and sample 2 was specially prepared for the current experiments aiming for a highest concentration of ferromagnetic Fe atoms in an amorphous state. Sample 5 is the identical sample previously studied by Mook and Tsuei,[3] who kindly provided us with the sample. Most of the measurements were made on sample 5 since it was the one in which a large magnon energy gap had been reported.

II. EXPERIMENTAL

The measurements were carried out at a triple-axis spectrometer at the high-flux beam reactor at Brookhaven National Laboratory with the configuration illustrated in Fig. 2(a). Sample S is exposed to an unpolarized beam from a monochromator, pyrolytic graphite (002). The horizontal magnetic field of 7.5 kOe is applied along the scattering vector Q, then the neutron polarization is rotated to the vertical position by a guide magnet. The flipper is placed just before the analyzer, Heusler (111).

This geometry is inverse to the conventional set-up in which polarized neutrons are created at the monochromator and the energy analysis is done either by the time-of-flight (TOF) technique or by a nonpolarizing crystal analyzer. The procedure of the measurement is identical in both setups. As shown in Fig. 2(b), for a single-crystal sample of Heusler alloy the OFF and ON channels cleanly pick up the expected magnetic excitation. Note that the Heusler (111) analyzer reflects (−) neutrons when the flipper is off, in contrast to an Fe polarizer where the channels are reversed. For the study of amorphous ferromagnets, where we expect large elastic scattering as well as nonmagnetic inelastic cross sections, we take the difference of OFF and ON counts. This process should eliminate all but magnetic inelastic cross sections and we expect the curve to go through zero at the elastic position. However, this simple picture can be distorted by a polarization effect which we will describe later.

We should point out in passing that the inverse geometry has a considerable intensity advantage over the more conventional polarizer-sample-graphite arrangement. This is due to the fact that the sample-counter distance is usually considerably shorter than the sample-source distance. Even standard magnetic form-factor measurements may benefit by using this arrangement for a good signal with a low background.

TABLE I. Magnetic properties of amorphous ferromagnets.

	Samples			
	1	2	5	4
Composition	$(Fe_{93}Mo_7)_{80}B_{10}P_{10}$	$Fe_{84}B_{16}$	$Fe_{75}P_{15}C_{10}$	Fe ingot
T_c	450 K	620 K	600 K	1042 K
μ_B/Fe atom at 295 K	$\sim 1\mu_B$	$1.8\mu_B$	$1.8\mu_B$	$2.2\mu_B$
D meV^2 Å at 295 K	68	140	149	280
Effective thickness	~2 mm	~2 mm	~1 mm	6 mm (0.6 mm)
Transmission-polarization effect at 30 meV[a]	0.6%	2.2%	3.4%	20% (2%)
Correction factor at 30 meV[b]	<0.2%	~1%	~1.3%	~15%

[a]Defined as the fractional increase in transmission of one polarization state relative to the other.

[b]Empirical effective transmission-polarization factor necessary to antisymmetrize (OFF−ON) counts around $\Delta E=0$ (see text).

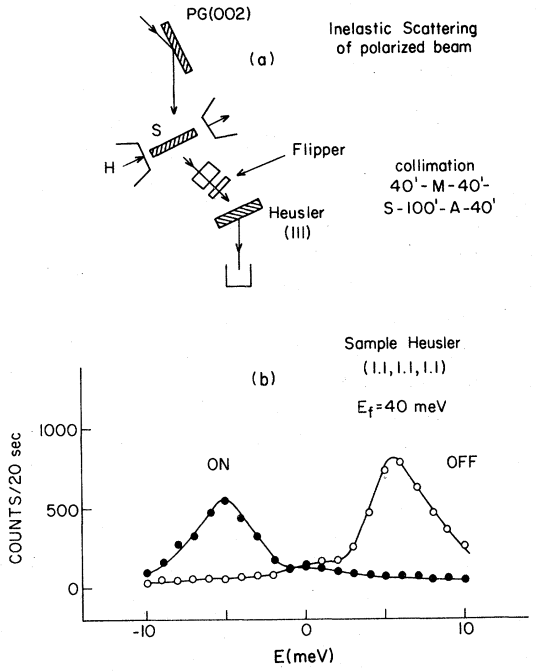

FIG. 2. (a) Experimental setup of polarized-beam triple-axis spectrometer. Sample S is placed in a horizontal magnetic field of 7.5 kOe. (b) Test of overall efficiency by using magnons from a Heusler single crystal at room temperature.

We have limited our measurements to the range of final energy E_f from 24 to 60 meV, and an energy transfer of 15 meV. This is simply a matter of intensity and counting time. The TOF technique[3,6] is far more efficient than the triple-axis polarized-beam spectrometer for this type of measurement. We emphasize that we are only concerned with the cross sections at low energy transfer.

All of our samples are placed in an aluminum container with an area of 25×25 mm^2. The collimators are all 40 min except for 100 min between sample and analyzer. The overall polarizing efficiency was tested by placing a matching Heusler (111) at the sample position in a vertical field. The flipping ratio ranges between 15 and 40 for the experimental conditions employed. The data shown in Fig. 2(b) demonstrates the proper functioning of the system.

In order to properly compare the data on these amorphous samples, we have characterized them further under identical conditions by performing conventional unpolarized small-angle magnon studies as shown in Fig. 3.

III. MAGNETIC CROSS SECTIONS NEAR $\mathcal{S}(Q)$ MAXIMUM

Figure 1(a) shows a typical elastic scattering $\mathcal{S}^0(Q)$ of amorphous ferromagnets. Actually, these data were taken with the analyzer set at 30 meV. We have selected most of our inelastic scans with the constant $Q_0 3.05$ Å^{-1}. This Q is close enough to the $\mathcal{S}^0(Q)$ maximum and avoids contamination from the Al(200) peak. Selected scans were also carried out with constant E configurations. Magnetic excitations were clearly observed as the difference of OFF and ON counts and clearly peaked near $Q=Q_0$ as found by Mook and Tsuei. These are, however, less than 10% of the total inelastic cross sections, thus, a very long counting time was required to accumulate adequate statistics.

Let us now examine more closely the observed intensities. The data for sample 1, $(Fe_{95}Mo_7)_{80}B_{10}P_{10}$, are shown in Fig. 4; the upper part depicts average counts of OFF and ON channels normalized to 1% of the counting time for obtaining the difference

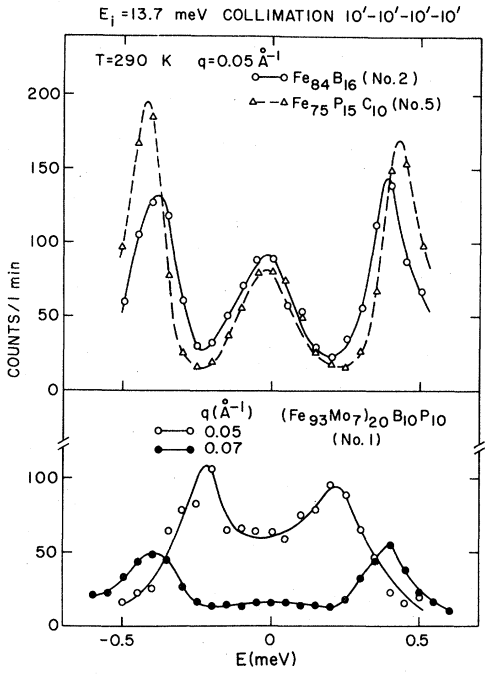

FIG. 3. Characterization of three amorphous ferromagnets at room temperature. All of the small-angle magnon data were taken with the identical experimental conditions. Note that magnon intensities of sample 1 are weaker (at the same energy) in comparison with the other two samples.

counts, except at the upper end where they are scaled to 10% counting time. These are comparable to the observed-difference cross section. The profiles of the average intensity represent the energy resolution at this energy. We could not extend our measurements beyond the energy transfer of -5 meV (neutron energy gain) because the horizontal magnets interfere with the scattering arm carrying the flipper. We note that the difference counts OFF$-$ON go through zero near the elastic position as expected.

We observed peaks at ~ 2 meV, both energy loss and energy gain. As we will see later, these peak positions are consistent with the resolution effect and they do not necessarily signify an energy gap. The peak position shifts to higher energies when we increase E_f from 30 to 60 meV reaching around 6 meV. The identical sample was studied by the correlation technique[7] with $E_i = 120$ meV (and correspondingly coarser resolution) and the peak observed around 11 meV, also approximately what one would expect from resolution. We thus conclude that a gap may exist but it is not detectable under the current experimental conditions if it is smaller than 2 meV.

The data for the Mook-Tsuei sample 5, $Fe_{75}P_{15}C_{10}$, gave an entirely different appearance at first glance as shown in Fig. 5. The OFF$-$ON differences do not show an expected antisymmetric shape which goes through zero at the elastic position. Instead, they exhibit a sharp peak near $\Delta E = 0$, the characteristic shared with another amorphous sample 2, ($Fe_{84}B_{16}$). In order to resolve this unexpected extra component we have carried out a series of tests comparing the amorphous samples and polycrystalline Fe ingots of various thicknesses. As demonstrated below, this is due to a beam-polarization effect within the sample, an effect known for many years.[8]

First, we measured the polarization of the unscattered beam after transmission through the sample. In Fig. 2(a) we set the Heusler analyzer at $2\theta_S = 0$ and measured the OFF$-$ON difference. As listed in Table I, samples 2 and 5 show considerably larger polarization effects than No. 1, while the Fe ignots clearly demonstrate the thickness dependence of this effect. The $(+)$ neutrons (detected at the ON position) are more efficiently scattered out than the $(-)$ neutrons by the sample; thus the sample, on the average, is irradiated by a larger number of $(-)$ neutrons. This is a relatively minor effect of the order of a few percent at most and is inconse-

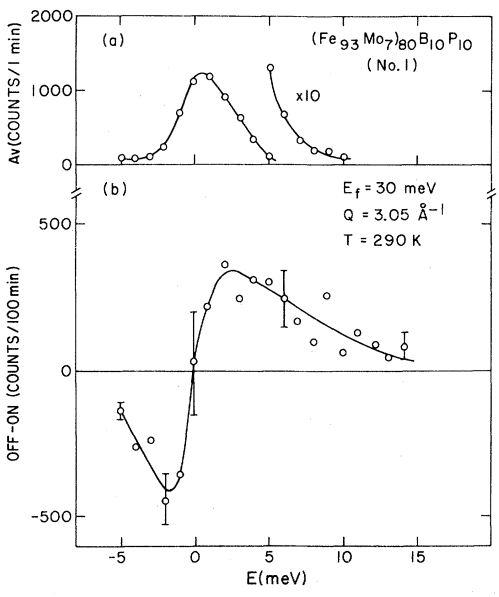

FIG. 4. Difference counts OFF$-$ON for $(Fe_{93}Mo_7)_{80}B_{10}P_{10}$ are shown in (b). The data near zero energy transfer are average from repeated runs. The average counting rates of OFF and ON are shown in (a) for 100 times shorter time.

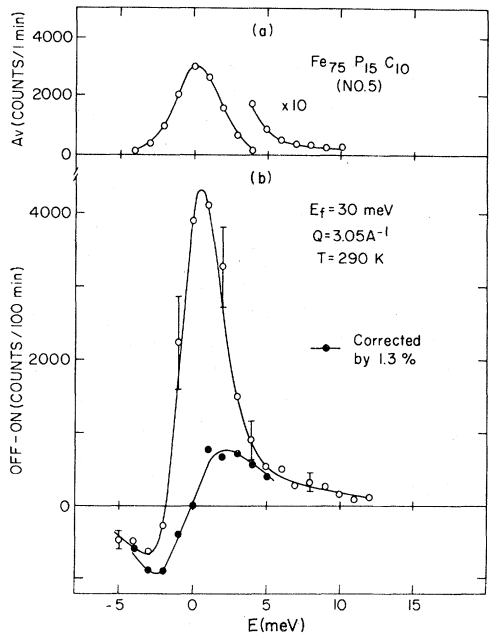

FIG. 5. Identical data presentation with Fig. 4 for the Mook-Tsuei sample $Fe_{75}P_{15}C_{10}$. The sharp peak around zero energy transfer is due to a transmission-polarization effect (see text).

quential in regular scattering experiments. This becomes a very serious correction when we take the differences of two large numbers near $\Delta E = 0$. As shown in Fig. 5, the central elastic (mostly nuclear) component is 100 times larger than the difference counts.

We have so far failed to find an analytic prescription for correcting the data for this polarization effect. If we directly apply a 3% correction (the value obtained from the transmission measurements), the difference peak on the positive side is considerably overcorrected. This is qualitatively understandable since the OFF−ON transmission difference may include additional spin-flap effects. We then adopted an empirical approach by assuming that the effective absorption correction must bring the difference count to zero at $\Delta E = 0$. This entails reducing the (−) neutron counts by 1.3% before taking the difference. The corrected data are shown by solid circles in Fig. 5(b).

This same empirical approach discussed above fails at $E_f = 60$ meV. Subtraction of a constant fraction of the measured quasielastic cross section [solid line, Fig. 6(a)] from the raw magnetic scattering [Fig. 6(b), solid line] does not produce the required antisymmetric line shape. However, interestingly enough, an acceptable antisymmteric line shape [dashed curve, Fig. 6(b)] results by subtracting from the raw data of Fig. 6(b) a constant (1%) fraction of the "elastic" component of Fig. 6(a) (i.e., the dashed curve with the intrumental linewidth). We have no detailed justification for this *ad hoc* procedure. But note in this regard that the observed quasielastic linewidth is significantly larger than the resolution linewidth at 60 meV, in contrast to the case for the 30-meV data. This presumably reflects the increased contribution of inelastic processes due to poorer resolution at high energies.

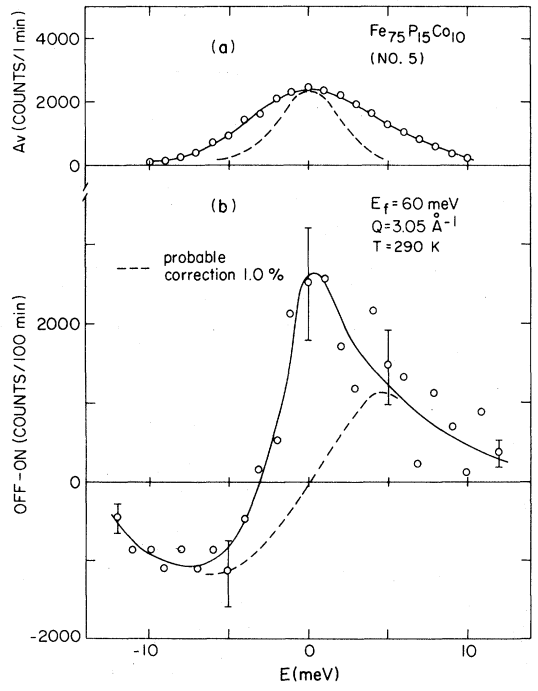

FIG. 6. Energy dependence of the data for $Fe_{75}P_{15}C_{10}$. Note the transmission-polarization correction is somewhat smaller for higher energy of $E_F = 60$ meV.

We have tried to prove this transmission-polarization effect by the measurements on Fe ingots, where all cross sections are known. With a large 2−6 mm thickness the polarization effects are so dominant that it was not possible to extract meaningful cross sections. With decreasing thickness the magnon intensities decreased; no suitable experimental "windows" were found for Fe which has a sharp strong elastic peak and a very large stiffness constant D.

We have to resolve one more question about the polarization correction. Why is the polarization correction much smaller in sample 1 which shows a magnon cross section (see Fig. 3) approximately 50% smaller than that of sample 5, but has a central component at least six times weaker? This is probably due to the fact that the spin-wave cross section is proportional to $\langle S \rangle$ at low temperatures ($T \ll T_c$) while the polarization effect is proportional to $\langle S \rangle^2$ at room temperature. We made the transmission measurement of sample 1 as a function of temperature, and it shows an increase from 0.6% at room temperature to 1.2% at 10 K.

IV. DISCUSSION

While thinking about inelastic magnetic scattering measurements at large momentum transfer it is important to keep in mind the possible distinction between the momentum transfer at the scattering event $\vec{Q}$ and the momentum of the excitation $\vec{q}$ so produced. The distinction is clear in crystalline systems where the two may differ by any lattice-reciprocal-lattice vector $\vec{Q} - \vec{q} = \vec{G}_{hkl}$. In this "umklapp" scattering the deficit momentum is taken up by the lattice as a whole. It is less widely realized that essentially identical processes occur in amorphous solids as well.[9,10] Neutron scattering measurements unambiguously establish that spin waves with a well defined momentum $\vec{q}$ occur for sufficiently long wavelengths, $\vec{q} < q_m \ll (2\pi/d)$ where d

represents the interatomic spacing. It it therefore essential to understand to what extend these small q excitations contribute to the higher momentum neutron scattering.

The expression for the appropriate generalization of umklapp ferromagnetic spin-wave scattering for a monoatomic amorphous solid is derived in the Appendix,

$$\mathcal{S}^{\pm}_{\rm sw}(\vec{Q},\omega)=2S\lambda(Q)\sum_{|q|<q_m}(n_q+1)\times\mathcal{S}^0_n(\vec{Q}-\vec{q})\delta(\omega-Dq^2)\,. \tag{1}$$

Equation (1) represents a convolution of the spin-wave spectrum with the elastic nuclear-structure factor

$$\mathcal{S}^0_n(\vec{Q})=N^{-1}\sum_l e^{-2w(Q)}e^{i\vec{Q}\cdot\vec{l}}\,.$$

From the form of the expression it is clear that one expects to see scattering due to the $q<q_m$ spin waves centered about those values of $\vec{Q}$ for which $\mathcal{S}^0_n(\vec{Q})$ is sharply peaked. The subscript sw reminds us that this is only a portion of the total magnetic inelastic cross section that has to do with well defined wave vectors $|q|<q_m$. There are *conceivably* other sharp contributions to $\mathcal{S}^{\pm}(\vec{Q},\omega)$ at large $\vec{Q}$ which represent new physics.[4] But *certainly* $\mathcal{S}^{\pm}(Q,\omega)$ contains $\mathcal{S}^{\pm}_{\rm sw}(\vec{Q},\omega)$. Equation (1) does not represent simply a replication of the long-wavelength spin waves. To see what is implied it is only necessary to carry out the convolution indicated in Eq. (1). This is performed in Appendix I. The essentials of the result can be most easily grasped by approximating $\mathcal{S}^0_n(\vec{Q})$ by an infinitesimal spherical shell,

$$\mathcal{S}^0_n(\vec{Q})=\delta(|\vec{Q}|-Q_0)\,.$$

This is equivalent to a polycrystalline approximation, for which

$$\mathcal{S}_{\rm sw}(|\vec{Q}|,\omega)\begin{cases}\sim\dfrac{S\lambda(Q)}{D}\left[\dfrac{Q_0}{Q}\right][n(\omega)+1], & |\omega|>D(Q-Q_0)^2\\ =0, & |\omega|<D(Q-Q_0)^2\,.\end{cases} \tag{2}$$

Because of the smearing due to rotational averaging, the scattering is not sharply defined in $\vec{Q}$ but is constrained to lie within and smoothly fill a volume bounded by a parabolic surface of revolution [Fig. 7(a)]. There is, of course, no gap in this spectrum.

We have tested this umklapp model to see whether it is consistent with our observations of the magnetic scattering seen around the first elastic diffraction maximum. This was done by convoluting

$$\mathcal{S}^{\pm}_{\rm sw}(|Q|,\omega)-\mathcal{S}^{\mp}_{\rm sw}(|Q|,\omega)$$

given by Eqs. (A5) and (A6) with the appropriate instrumental resolution functions for several typical cases. Some results are shown in Figs. 8 and 9. For the "amorphous" case we have approximated $\mathcal{S}^0_n(|Q'|)$ by a triangular function with the observed full width at half maximum (FWHM). The "polycrystalline" approximation was discussed above.

To recapitulate the essential points of the umklapp model one begins with the established fact of well-defined spin-wave excitations at small wave vectors. These excitations cause scattering around the first diffraction maximum at Q_0 (and subsequent maxima as well) but with an altered (diffuse) momentum distribution [Fig. 7(a)]. At Q_0 this gives rise to $\mathcal{S}^{\pm}-\mathcal{S}^{\mp}$ shown in Fig. 7(b) (assuming no intrinsic spin-wave damping). With finite spectrometer resolution, which increases with increasing E_f, the observed intensity differences show apparent gaps [Fig. 7(c)].

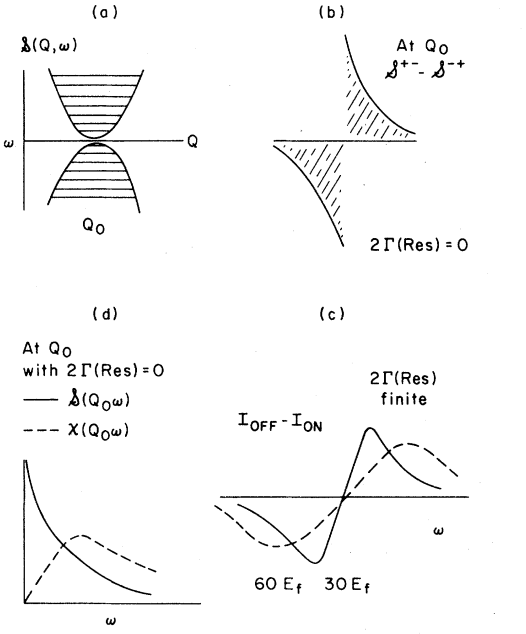

FIG. 7. Schematic presentation of magnon measurements by the polarized-beam technique. (a) We assume a simple cross section (with no gap) around the $\mathcal{S}(Q)$ maximum Q_0. (b) With ideal resolution condition ($2\Gamma=0$), $\mathcal{S}(Q_0,\omega)$ peaks at $\omega=0$ but $\chi(Q_0,\omega)$ ($\simeq\mathcal{S}\omega$) show a peak at finite ω. (c) OFF—ON counts remove phonons and elastic components and diverge at $\omega=0$. (d) Finite resolutions create a peak in OFF—ON counts.

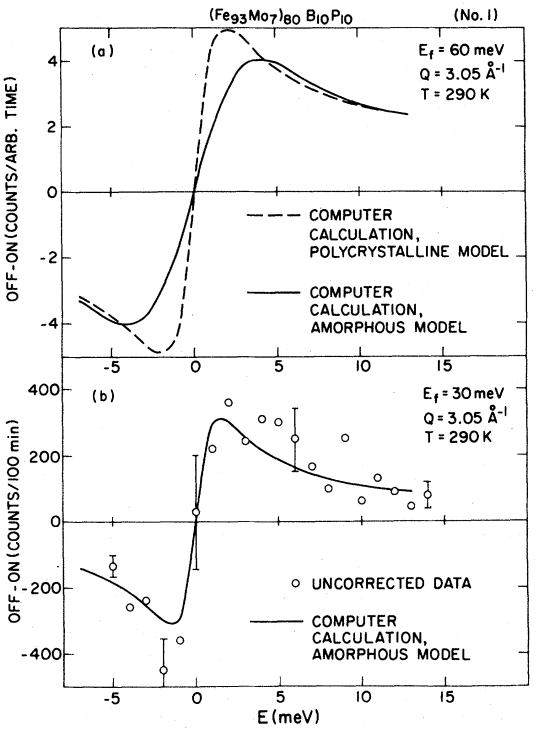

FIG. 8. Numerical calculation of $[\mathcal{S}^{\pm}_{sw}(|Q|,\omega) - \mathcal{S}^{\mp}_{sw}(|Q|,\omega)]$ described in the text for sample 1 convoluted with the appropriate spectrometer resolution function is plotted as a function of energy. In (a) the polycrystalline model is compared to the amorphous model for a final neutron energy of 60 meV. In (b) the amorphous model is compared directly to uncorrected experimental data for a final neutron energy of 30 meV.

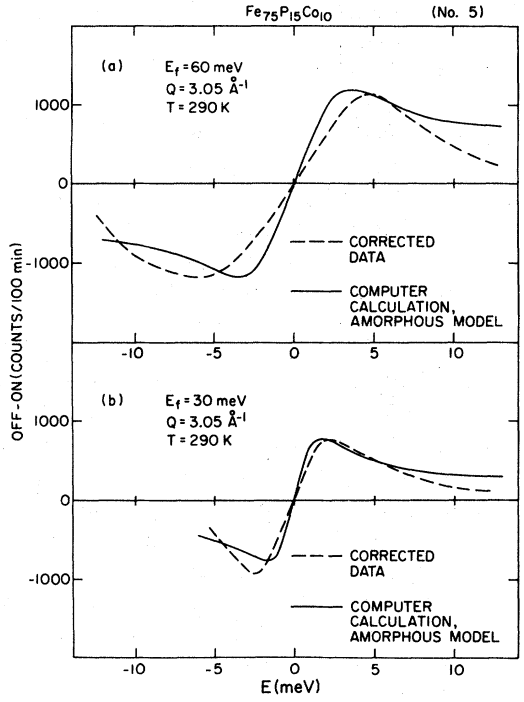

FIG. 9. Numerical calculation of $[\mathcal{S}^{\pm}_{sw}(|Q|,\omega) - \mathcal{S}^{\mp}_{sw}(|Q|,\omega)]$ for sample 5 according to the amorphous model described in the text convoluted with the appropriate instrumental resolution function is compared to corrected experimental data for a final neutron energy of (a) 60 meV and (b) 30 meV.

There is one other very important feature of the Mook-Tsuei result which should be emphasized. They chose to present

$$\chi''(Q,\omega) = [n(\omega)+1]^{-1}\mathcal{S}_m(Q,\omega)$$

rather than $\mathcal{S}_m(Q,\omega)$. Since for $\hbar\omega \ll kT$, $\chi''(Q,\omega) \approx (\hbar\omega/kT)$, $\mathcal{S}_m(Q,\omega)$ is odd in ω and shows a peak at finite ω even if $\mathcal{S}_m(Q,\omega)$ does not [see Fig. 7(d)]. Furthermore, a peak in $\chi''(Q,\omega)$ does not necessarily imply a gap. [Consider, for example, a simply Debye relaxation for which $\chi(\omega) \sim (1-i\omega\tau)^{-1}$ (Ref. 11).] Mook and Tsuei's $\chi''(Q,\omega)$ when converted to $\mathcal{S}(Q,\omega)$ shows no peak at finite ω, as shown in Fig. 1(c), and we can speculate that they might have reached a very different conclusion concerning a gap if they had been looking at $\mathcal{S}(Q,\omega)$ rather than $\chi''(Q,\omega)$. Another equally important point is that in converting observed intensity into $\chi''(\vec{Q},\omega)$ [or $\mathcal{S}(\vec{Q},\omega)$] one must be careful to first remove resolution effects which can cause considerable distortion [Fig. 7(c)].

Finally, we would like to comment on the expression "a rotonlike," used in conjunction with excitations in amorphous ferromagnets. In the umklapp model discussed above $\mathcal{S}^{\pm}_{sw}(\vec{Q},\omega)$ had features reminiscent of rotons in superfluids but it seems unnecessary and possibly misleading to pursue them. The dynamics of $\mathcal{S}^{\pm}_{sw}(\vec{Q},\omega)$ is only that of the long-wavelength spin waves. We believe that our data are satisfactorily explained by $\mathcal{S}^{\pm}_{sw}(\vec{Q},\omega)$. It is not clear that the Mook-Tsuei data, which principally explore larger energy transfer than was possible in these experiments, can be explained by $\mathcal{S}^{\pm}_{sw}(\vec{Q},\omega)$.

The more basic question of a rotonlike behavior is whether the amorphous ferromagnets have a genuine energy gap at Q_0 and this is the question we are reexamining in this paper. Alben[9] states his opinion that a rotonlike dip in amorphous ferromagnets is explained "in terms of static structural correlations rather than dynamical effects." Alben's results do not give a peak in $\mathcal{S}_{mag}(\vec{Q}_0,\omega)$ as a function of ω, although they would produce a peak

qualitatively similar to those reported by Mook and Tsuei in $\chi''(Q,\omega)$.

The triple-axis data described above fall short of providing a complete quantitative picture of low-energy magnetic excitations near the $\mathcal{S}(Q)$ maximum in amorphous ferromagnets. They do point out, however, two important features not previously discussed. One is the resolution effect which automatically creates an apparent gap. Another is the transmission-polarization effect which distorts cross sections near $\Delta E=0$. Obviously, one must carry out the orthodox inelastic polarized-beam experiment with polarization analysis in order to lower the upper limit of the gap below 2 meV. This is planned in the near future.

Very recently, we were informed by Cowley of new triple-axis measurements[12] on an amorphous sample very similar to our sample 2. They apparently also reached the conclusion of "no gap" through somewhat different reasoning. We feel it is important that independent measurements are being carried out to clarify this important question in amorphous ferromagnets.

Note added. After this manscript was submitted Mook informed us that he has reexamined $Fe_{75}P_{15}C_{10}$ at improved signal-to-noise ratio with his time-of-flight instrument. The data taken near Q_0 show considerable scattering at small energy transfer in qualitative agreement with what we have identified in this paper as umklapp scattering from long-wavelength spin waves. These new data extend considerably beyond the 10-meV energy transfer studied here, and when presented as $\chi''(Q_0,E)$, show a broad peak at ~ 17 meV.

ACKNOWLEDGMENTS

We would like to thank H. A. Mook and C. Tsuei for kindly providing us with their sample and R. A. Cowley, H. A. Mook, K. Motoya, and S. M. Shapiro for many stimulating discussions. We are also very grateful to N. Akutsu of Gakushuin University for a very skillful preparation of a new amorphous sample for the current study. The work at Brookhaven National Laboratory was carried out under the Division of Basic Energy Sciences, U.S. Department of Energy, Contract No. DE-AC02-76CH00016.

APPENDIX: UMKLAPP SCATTERING IN AMORPHOUS SOLIDS

We will examine explicitly the case of ferromagnetic spin waves in a monatomic solid although the principle applies equally to other long-wavelength excitations (e.g. acoustic phonons). Assuming that the spin and positional degrees of freedom are independent, the transverse magnetic inelastic scattering is given by

$$\mathcal{S}_{\rm mag}(\vec{Q},\omega)=\mathcal{S}^{\pm}(\vec{Q},\omega)+\mathcal{S}^{\mp}(\vec{Q},\omega)\ ,$$

where

$$\mathcal{S}^{\pm}(\vec{Q},\omega)=\lambda(Q)\sum_l e^{-2W(Q)}e^{i\vec{Q}\cdot\vec{l}} \times\int\langle S_0^{+}(0)S_l^{-}(t)\rangle \times e^{i\omega t}dt\ , \tag{A1}$$

where $S_l^{\pm}(t)$ is the time-dependent spin variable on the atom at vector position $\vec{l}$, and $\lambda(\vec{Q})$ is the square of the neutron-spin coupling constant. The spin-spin correlation function even in the one-magnon approximation is not simple for an amorphous material, but we know that there is a macroscopic limit in which q is much smaller than (interatomic spacing)$^{-1}$ for which simple spin waves should be appropriate. This contribution is readily evaluated,[13]

$$\int\langle S_0^{+}(0)S_l^{-}(t)\rangle e^{i\omega t}dt =\frac{2S}{N}\sum_{\vec{q}(|q|<q_m)}(n_q+1)e^{i\vec{q}\cdot\vec{l}}\delta(\omega-\omega_q)+\cdots\ , \tag{A2}$$

where the ellipsis stands for contributions from other long-wavelength spin waves.

The spin-wave contribution to $\mathcal{S}^{\pm}(\vec{Q},\omega)$ is

$$\mathcal{S}^{\pm}_{\rm sw}(\vec{Q},\omega) =2S\lambda(Q)\sum_{|q|<q_m}(n_q+1)\delta(\omega-Dq^2) \times\sum_l N^{-1}e^{-2W(Q)}e^{i(\vec{Q}-\vec{q})\cdot\vec{l}}\ ,$$

which leads, by definition of $\mathcal{S}_n^0(\vec{Q})$, to Eq. (1).

The corresponding expression for the long-wavelength spin-wave contribution to $\mathcal{S}^{\mp}(\vec{Q},\omega)$ is

$$\mathcal{S}^{\mp}_{\rm sw}(\vec{Q}\omega)=2S\lambda(Q) \times\sum_{|q|<q_m}n_q\mathcal{S}_n^0(\vec{Q}-\vec{q})\delta(\omega+Dq^2)\ . \tag{A3}$$

In order to further simplify Eqs. (1) and (A3) we use the fact that $\mathcal{S}_n^0(\vec{Q}')$ depends only upon the magnitude of $\vec{Q}'$ and that ω_q likewise depends only on the magnitude of $\vec{q}$ to rewrite Eq. (1) as

$$\mathcal{S}^{\pm}_{\rm sw}(|Q|,\omega)=2S\lambda(Q)[n(\omega)+1]\times\sum_{Q'}\mathcal{S}^{0}_{n}(|Q'|)\rho_{Q'}(\omega)\,, \quad \text{(A4)}$$

where now $\vec{Q}'=\vec{Q}-\vec{q}$ and $\rho_{Q'}(\omega)$ is the density of states with frequency ω and umklapped wave vector Q'. This latter is proportional to the area of a circular annulus formed by wave vectors $|q|$ on a sphere of radius Q' (see Fig. 10).

Therefore,

$$\rho_{Q'}(\omega)d\omega\sim hQ'd\phi=Q'^2\sin\phi d\phi$$

or

$$\rho_{Q'}(\omega)\sim Q'^2\sin\phi\left|\frac{d\phi}{dq}\right|\left|\frac{dq}{d\omega}\right|=\frac{1}{2D}\frac{|Q'|}{|Q|}\,, \quad \text{(A5)}$$

where we have used the relation

$$q^2=Q'^2+Q^2+2Q'Q\cos\phi\,.$$

Equation (A5) is correct as long as $\vec{q}$ can form a triangle with $\vec{Q}$ and $\vec{Q}'$, which are considered fixed; i.e., as long as $|q|>|Q'-Q|$, or equivalently for $|\omega|D(Q'-Q)^2$. Substituting into Eq. (A4) we find

$$\mathcal{S}^{\pm}_{\rm sw}(|Q|,\omega)\begin{cases}\sim\dfrac{S\lambda(Q)}{D}(n(\omega)+1)\\ \times\displaystyle\sum_{|Q'|}{}'\,\mathcal{S}^{0}_{n}(|Q'|), & \omega>0\\ =0, & \omega<0\end{cases} \quad \text{(A6)}$$

where the prime indicates that Q' must be such that

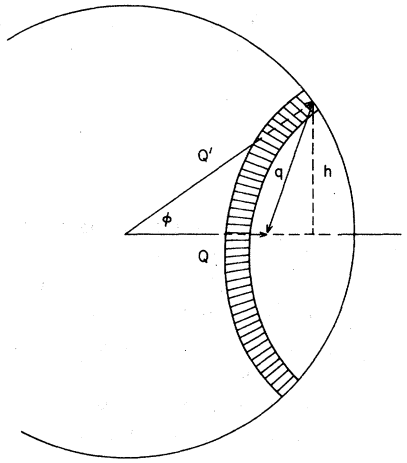

FIG. 10. Geometry used in "powder averaging" the scattering cross section. For any given nominal wave vector $|\vec{Q}|$ there are degenerate contributions from many umklapped wave vectors $\vec{q}$ whose number is proportional to the shaded annulus.

$|\omega|>D(Q'-Q)^2$. Similarly,

$$\mathcal{S}^{\mp}_{\rm sw}(|Q|,\omega)\begin{cases}\sim\dfrac{S\lambda(Q)}{D}n(|\omega|)\\ \times\displaystyle\sum_{|Q'|}{}'\,\mathcal{S}^{0}_{n}(|Q'|), & \omega<0\\ =0, & \omega>0\,.\end{cases} \quad \text{(A7)}$$

Setting $\mathcal{S}^{0}(|Q'|)=\delta_{Q',Q_0}$ leads immediately to the results quoted in Eq. (2).

[1]R. M. Moon, T. Riste, and W. C. Koehler, Phys. Rev. 181, 920 (1969).

[2]H. A. Mook, N. Wakabayashi, and D. Pan, Phys. Rev. Lett. 34, 1029 (1975).

[3]H. A. Mook and C. Tsuei, Phys. Rev. B 16, 2184 (1977).

[4]Y. Takahashi and M. Shimizu, Phys. Lett. A 58, 419 (1976).

[5]J. D. Axe, G. Shirane, T. Mizoguchi, and K. Yamauchi, Phys. Rev. B 15, 2763 (1977).

[6]K. Motoya, M. Nishi, Y. Ito, and T. Mizoguchi, J. Phys. Soc. Jpn. 49, 115 (1980).

[7]C. F. Majkrzak and H. A. Mook (unpublished). Data were taken at the Oak Ridge TOF machine at 50 K. At this temperature $\chi(Q,\omega)$ are not drastically different from $\mathcal{S}(Q,\omega)$ above 5 meV.

[8]See, for example, G. E. Bacon, *Neutron Diffraction* (Clarendon, Oxford, 1975).

[9]R. Alben, in *Magnetism and Magnetic Materials—1975 (Philadelphia)*, Proceedings of the 21st Annual Conference on Magnetism and Magnetic Materials, edited by J. J. Becker, G. H. Lander, and J. J. Rhyne (AIP, New York, 1976), p. 136. The calculated contours labeled $\mathcal{S}(Q,\omega)$ in this paper are actually $\chi''(Q,\omega)$ since the thermal occupation number was neglected. They agree qualitatively with the experimentally χ'' by Mook and Tsuei.

[10]J. D. Axe, in *Physics of Structurally Disordered Materials*, edited by S. S. Mitra (Plenum, New York, 1976), p. 507.

[11]It was pointed out by J. M. Lawrence and S. M. Shapiro [Phys. Rev. B 22, 4379 (1980)] that if $\mathrm{Im}\chi(\omega)=A\Gamma\omega/(\omega^2+\Gamma^2)$ then $I(Q\omega)$ shows a peak at low-temperature limit because $n(\omega)+1\approx1$.

[12]R. A. Cowley (private communication); D. Paul, R. A. Cowley, N. Cowlam, and W. G. Stirling, J. Phys. F (in press).

[13]See, for example, G. L. Squires, *Introductory Theory of Thermal Neutron Scattering* (Cambridge University Press, Cambridge, England, 1978).